HHS Public Access

Author manuscript

Dev Biol. Author manuscript; available in PMC 2020 April 01.

Published in final edited form as:

Dev Biol. 2019 April 01; 448(1): 36–47. doi:10.1016/j.ydbio.2019.01.014.

Loss of the neurodevelopmental Joubert syndrome causing protein, Ahi1, causes motor and muscle development delays independent of central nervous system involvement

Justin R. Bourgeois[a] and **Russell J. Ferland**[a,b,*]

[a]Department of Neuroscience and Experimental Therapeutics, Albany Medical College, Albany, New York, USA, 12208

[b]Department of Neurology, Albany Medical College, Albany, New York, USA, 12208

Abstract

Joubert syndrome (JBTS) is a predominantly autosomal recessive neurodevelopmental disorder that presents with characteristic malformations of the cerebellar vermis, superior cerebellar peduncles and midbrain in humans. Accompanying these malformations are a heterogeneous set of clinical symptoms, which frequently include deficits in motor and muscle function, such as hypotonia (low muscle tone) and ataxia (clumsiness). These symptoms are attributed to improper development of the hindbrain, but no direct evidence has been reported linking these in JBTS. Here, we describe muscle developmental defects in a mouse with a targeted deletion of the *Abelson helper integration site 1* gene, *Ahi1*, one of the genes known to cause JBTS in humans. While FVB/NJ $Ahi1^{-/-}$ mice display no gross malformations of the cerebellum, deficits are observed in several measures of motor function, strength, and body development. Specifically, $Ahi1^{-/-}$ mice show delayed physical development, delays in surface reflex righting as neonates, and reductions in grip strength and spontaneous locomotor activity as adults. Additionally, $Ahi1^{-/-}$ mice showed evidence of muscle-specific contributions to this phenotype, such as reductions in 1) myoblast differentiation potential *in vitro*, 2) muscle desmin expression, and 3) overall muscle mass, myonuclear domain, and muscle fiber cross-sectional area. Together, these data suggest that loss of *Ahi1* may cause abnormalities in the differentiation of myoblasts to mature muscle cells. Moreover, *Ahi1* loss impacts muscle development directly, outside of any indirect impact of cerebellar malformations, revealing a novel myogenic cause for hypotonia in JBTS.

Keywords

Joubert syndrome; Ahi1; hypotonia; myogenic; desmin

[*]Correspondence to: Russell J. Ferland, Ph.D. Albany Medical College Department of Neuroscience and Experimental Therapeutics 47 New Scotland Avenue, MC-136 Albany, NY 12208 Phone: (518) 262-0172 Fax: (518) 262-5799, ferlanr@amc.edu.

Introduction

Joubert syndrome (JBTS) is a neurodevelopmental disorder with an estimated prevalence of 1/80,000 live births (Brancati et al., 2010; Romani et al., 2013), although this may be an underestimate. The main neuroanatomical characteristic of JBTS is a pathognomonic MRI finding termed the “molar tooth sign” (MTS), comprising aplasia or hypoplasia of the cerebellar vermis, thickened and elongated superior cerebellar peduncles (SCPs; including failure to decussate), and a deepened interpeduncular fossa (Brancati et al., 2010; Ferland et al., 2004; Maria et al., 1997). Accompanying these MRI findings is a heterogeneous collection of symptoms, which most frequently include hypotonia, respiratory disturbances, developmental delay, ataxia, ocular motor apraxia, and varying degrees of cognitive impairment (Brancati et al., 2010; Romani et al., 2013). Additional symptoms may include retinal degeneration, renal defects, polydactyly, and failure to thrive (Brancati et al., 2010; Edvardson et al., 2010; Koshy et al., 2010; Parisi et al., 2007; Romani et al., 2013; Tunovic et al., 2015; Weiss et al., 2009). To date, more than 30 genes have been identified as a cause for JBTS, accounting for ~62–94% of known cases (Parisi and Glass, 1993 [updated 2017]). One such gene, the *Abelson helper integration site 1* gene (*AHI1*) was identified as a cause of JBTS (Ferland et al., 2004, Dixon-Salazar et al., 2004), and is responsible for ~7–10% of cases (Parisi and Glass, 1993 [updated 2017]), making it one of the most commonly identified genes in JBTS.

Although deficits involved in motor and/or muscle function are among the most frequently noted symptoms in JBTS, little is known about how the development of the muscular system may be directly affected in individuals with JBTS. These deficits are frequently characterized as being purely neurological in origin (Romani et al., 2013), however no experimental evidence exists to determine whether muscle development may be impacted directly by mutations in JBTS genes. While any mutations affecting central nervous system (CNS) development can be expected to play a role in motor function and muscle development, it is premature to exclude the possibility that mutations in causative JBTS genes may also impact the muscular system via a non-CNS mediated mechanism. Indeed, within the spectrum of observed JBTS phenotypes, deficits are present in multiple organs with no proposed link to CNS development, as evidenced by the presence of kidney, liver, skeletal, and congenital heart defects (Dempsey et al., 2017; Parisi et al., 2007; Romani et al., 2013; Strongin et al., 2018).

Currently existing data utilizing mouse models of Ahi1 loss present a complex picture of CNS involvement or non-involvement in motor function and muscle development. Interestingly, *AHI1*/*Ahi1* mRNA has been observed in both human and rodent skeletal muscle tissue (Prior et al., 2010), suggesting a possible role for AHI1 in muscle development. Moreover, published data utilizing brain-specific conditional $Ahi1^{-/-}$ mice show discrepancies between neonatal lethality (Louie et al., 2010), body development, and locomotor activity (Weng et al., 2013; Xu et al., 2010) when compared to global $Ahi1^{-/-}$ mice on the same background strain, indicating that these processes may be affected by the loss of Ahi1 in a CNS-independent fashion. We previously generated global $Ahi1^{-/-}$ mice (Hsiao et al., 2009), which have subsequently been backcrossed onto an FVB/NJ background to study the function of this gene in various aspects of development. While our

mice show reductions in body size, developmental delay, and deficits in measures of motor function, they show no evidence of gross cerebellar malformations as previously reported in another strain (Lancaster et al., 2011), indicating that these phenomena may be distinct. Here, we present evidence of intrinsic deficits in motor function and muscle development in FVB/NJ *Ahi1*$^{-/-}$ mice in the absence of an observable neuroanatomical phenotype.

Materials and Methods

Generation of *Ahi1*$^{-/-}$ mice

Previously generated C57BL/6J *Ahi1*$^{+/-}$ mice (*Ahi1*^{tm1Rujf}; (Hsiao et al., 2009)) were backcrossed at least 10 generations onto an FVB/NJ genetic background. *Ahi1*$^{-/-}$ and control mice were maintained from mating male and female *Ahi1*$^{+/-}$ mice. All mice were maintained on a 12 h light-dark cycle (07:00 to 19:00) with unlimited access to food and water. All mouse procedures were performed under approval from the Institutional Animal Care and Use Committee of Albany Medical College, in accordance with The National Institutes of Health *Guide for the Care and Use of Laboratory Animals*.

Embryonic and perinatal lethality analysis

Previous studies utilizing C57BL/6J *Ahi1*$^{-/-}$ mice demonstrated that *Ahi1*$^{-/-}$ mice rarely survived for more than 24 h (Hsiao et al., 2009). Therefore, litter size was observed at postnatal day 0.5 (PD0.5) in FVB/NJ *Ahi1* mice to determine total number of pups born, and were subsequently checked daily for neonatal lethality. For analysis of the effect of litter size on postnatal survival of *Ahi1*$^{-/-}$ pups, culled litters were reduced to a total of 6 pups at PD0.5.

Spontaneous locomotor activity

Prior to locomotor analyses, 7–9-week old mice were housed individually for a minimum of one week. At 12:00 on day 0, an individual mouse was placed in a 12” diameter Plexiglas cylinder with access to food, water, and bedding, within a larger closed chamber maintained on a 12 h light-dark cycle (07:00 to 19:00). Animals were allowed to acclimate to this environment for the remainder of the light cycle and the first dark cycle. Beginning at 07:00 on day 1, locomotor activity was recorded using Activity Monitor Software (Med Associates, Inc.) for 24 h.

Suspended weights test

Using a modified version of the suspended weights test (Deacon, 2013), weights with small metal handles were constructed weighing approximately 10, 19, 27, 36, 45, 54, 63, 72 and 81 g. Mice were lifted by the base of the tail and allowed to grasp the first weight with forepaws only. The mouse and weight were then lifted until the weight was suspended with a 3 sec hold ranked as a successful trial. Upon successful completion of one level, a mouse was scored 3 points (1 point/sec), then moved to the next level (increasing weight). Level increases were continued until the mouse was unable to hold a weight for 3 sec, with the longest of three failed attempts at the final level added to the total score.

Surface righting reflex assay

Mouse pups were placed upon their backs on a clean, flat surface, and prevented from moving until a stop clock was started. Upon release, the time for the mouse to reorient itself stably on all four paws was recorded. The result for an individual mouse was taken as an average of three trials. Mice were returned to their home cage for a resting period of five min between each trial.

Analysis of embryonic muscle tissue

Timed pregnant females were euthanized with pentobarbital when litters were at embryonic day (ED) 18.5. Embryos were extracted and euthanized, after which the skin was dissected from hindlimbs, and the upper posterior hindlimb muscle tissue was removed while on ice. Subsequently, tissue was placed in liquid nitrogen and stored at −80°C until homogenization was performed in pre-chilled RIPA lysis buffer (150 mM NaCl, 1.0% Triton X-100, 0.5% sodium deoxycholate, 0.1% sodium dodecyl sulfate (SDS), 50 mM Tris, pH 8.0) on ice. Homogenized samples were placed on a nutating mixer at 4°C for 45 min, followed by centrifugation at 16000 × g at 4°C for 15 min at which point the resulting supernatant was collected for analysis.

Analysis of brain tissue

Three week old and ten week old male mice were deeply anesthetized with pentobarbital and transcardially perfused with phosphate buffered saline (PBS), followed by ice-cold 4% paraformaldehyde (PFA) in PBS. Brains were immediately removed, weighed, and placed in 4% PFA overnight at 4°C. Brains were then rinsed three times in PBS and stored in 30% sucrose in PBS at 4°C. Once fully equilibrated, brains were cryosectioned at a thickness of 50 μm and stained with cresyl violet.

Immunolabeling of the SCP was performed on free-floating, 50 μm transverse brain sections from 10 week old male mice. Sections were rinsed with PBS before blocking in 1% BSA in 0.1% Triton X-100 PBS (PBS-Tx) for 1 h at room temperature (RT). Sections were then incubated overnight with sheep anti-myelin basic protein antibody (1:3000; Millipore, AB9046) in blocking buffer at 4°C. The following day, sections were rinsed 3 times for 20 min in PBS-Tx (0.1%) at RT, followed by 1 h incubation at RT with donkey anti-sheep Alexa Fluor 488 antibody (1:500; Invitrogen, A11015) in blocking buffer. Sections then underwent 3 times 20 min PBS-Tx (0.1%) rinses prior to mounting with Fluoromount G (Southern Biotech).

Brain section images were obtained with a Zeiss AxioImager.M2 upright microscope equipped with a Qimaging QIClick Camera (MBF Bioscience). Brain areas were measured using Neurolucida software (MBF Bioscience) with the sections blinded for genotype. Cerebellar areas were measured by manually tracing the outline of the cerebellum in both midline and paramedial sagittal sections. For whole brain area calculations, the forebrain was traced manually in both midline and paramedial sagittal sections up to a line that was drawn from the rostral boundary of the interpeduncular fossa to the most rostral edge of the fourth ventricle. To complete the whole brain calculation, the brain area rostral to this line

was traced and added to the previously measured cerebellar area resulting in the total brain area of midline and paramedial sagittal sections.

In vitro primary myoblast proliferation

PD1.5 *Ahi1*$^{+/+}$ and *Ahi1*$^{-/-}$ mice were euthanized, and under sterile conditions, muscle tissue was removed from the posterior upper hindlimb in ice cold PBS. Tissue was minced with razor blades and incubated in Dulbecco's Modified Eagle Medium (DMEM) supplemented with 300 U/ml type 2 collagenase and 2.5mM $CaCl_2$ for 45 min at 37°C. During this incubation, the cells were pipetted up and down 10 times every 15 min using a 1 ml serological pipette. Cells were then passed through a 100μm filter and centrifuged for 5 min at 350 × *g*, at which point cells were resuspended in proliferation medium (PM) (consisting of 1:1 F10/DMEM containing 20% fetal bovine serum (FBS), 1% penicillin/streptomycin, and 2.5 ng/ml basic fibroblast growth factor (bFGF)) and pre-plated for 20 min, three times on uncoated dishes to remove fibroblasts. The supernatant was then removed, after which cells were counted and seeded on 2% gelatin coated 35 mm dishes at 1.4 ×10^4 cells/cm^2 in PM. After 2 d, media was replaced either with fresh PM or differentiation medium (DM) consisting of DMEM containing 5% horse serum and 1% penicillin/streptomycin for 20 h, at which point media was replaced with identical media supplemented with 10 μM 5-bromo-2'-deoxyuridine (BrdU) for 4 h. Cells were then rinsed with PBS three times for 10 sec each, followed by two PBS rinses of 2 min each. Cells were then fixed with pre-chilled methanol at −20°C for 10 min, followed by three PBS rinses for 5 min each at RT. Cells were permeabilized with PBS-Tx (0.04%) for 5 min at RT, followed by three PBS rinses for 10 min each at RT. Cells were then treated with 2N HCl for 45 min at RT, followed by five PBS rinses for 5 min each at RT. Following incubation in blocking buffer consisting of 1% bovine serum albumin (BSA) in PBS at RT for 1 h, cells were incubated overnight at 4°C in mouse anti-BrdU antibody (1:200; Developmental Studies Hybridoma Bank (DSHB), G3G4) diluted in 1% BSA PBS. The following day, cells were rinsed three times in PBS for 10 min each at RT, followed by 1 h incubation at RT in anti-mouse secondary antibody (1:500; Invitrogen, A11030; goat anti-mouse IgG AlexaFluor 546). Cells were then rinsed three times in PBS for 10 min each, followed by a 1 min incubation in Hoechst 33258 (1μg/ml) and two subsequent rinses prior to being coverslipped with Fluoromount G.

Primary myoblast differentiation

Cells were initially harvested as described above, and grown for several passages in F10/DMEM PM on 1% collagen coated dishes with pre-plating performed at each passage to prevent fibroblast proliferation, at which point cells were switched to DMEM PM consisting of DMEM containing 20% FBS, 1% penicillin/streptomycin and 2.5 ng/ml bFGF. Cells were then seeded at 1.4 × 10^4 cells/cm^2 and allowed to reach ~70% confluence, at which point media was switched to DM. Cells were rinsed twice with ice cold PBS and collected in triplicate with RIPA lysis buffer upon reaching ~70% confluence (day 0), and at 3 d post-exposure to DM (day 3). Lysates were then placed on a nutating mixer for 30 min at 4°C followed by centrifugation at 16000 × g for 15 min at 4°C, at which point supernatants were collected for analysis.

Western blotting

Western blotting was performed as previously described (Hsiao et al., 2009). Briefly, lysate protein concentrations were determined using the Advanced Protein Assay (Cytoskeleton, Inc.). Samples were boiled in 2× Laemmli buffer for 5 min, and 35 μg protein per lane was loaded in 8% Tris/Glycine SDS polyacrylamide gels for separation at 100 V. Samples were then transferred to Immobilon-FL PVDF microporous membrane for 2 h on ice at 100V. Membranes were then blocked with 5% milk diluted in tris-buffered saline (TBS) + 0.1% Tween 20 (TBST) for 1 h at RT, followed by overnight incubation at 4°C with primary antibodies against desmin (1:100; DSHB, D3), myosin heavy chain (MHC) (1:200; DSHB, MF20) or GAPDH (1:10000; Abcam, ab9484) diluted in 3% milk TBST blocking solution. Membranes were then rinsed in TBST three times for 30 min each, followed by 1 h incubation at RT in secondary antibody (1:5000; Pierce, 32230, goat anti-mouse HRP) diluted in 3% milk TBST blocking solution. Immunodetection was performed using the Super Signal West Femto Maximum Sensitivity substrate kit (Thermo Scientific).

Muscle histology

Embryonic tissue was collected by euthanizing timed pregnant females with embryonic day (ED) 18.5 litters, at which point embryos were euthanized and transferred to ice cold PBS prior to dissection. Hindlimbs were skinned, removed, and placed into pre-chilled −20°C methanol overnight. The following day, hindlimbs underwent three 20 min PBS rinses at RT and were then placed into 30% sucrose in PBS for 48 h at 4°C to allow for cryoprotection. Hindlimbs were transferred to a cryostat to equilibrate for 30 min at −22°C prior to cryosectioning of 14 μm transverse sections. Postnatal tissue was collected by euthanizing mice at either 3 weeks or 3 months of age. Hindlimbs were removed and dipped in optimal cutting temperature (OCT) compound. Tissue was then flash frozen using liquid nitrogen cooled isopentane, placed on dry ice for 20 min to allow for evaporation of any liquid, and stored at −80°C. Prior to cryosectioning, samples were equilibrated in the cryostat for 1 h at −22°C. Sections were cut at a thickness of 14 μm (for P21 hindlimbs) or 50 μm (for 3 month old hindlimbs). Slides were allowed to air dry for 1 h prior to staining or storage at −20°C.

Muscle immunohistochemistry

Slides were rinsed in PBS to remove OCT compound, followed by incubation in blocking buffer (PBS-Tx (0.1%) supplemented with either 1% BSA (for anti-Na^+/K^+ ATPase subunit α1 (NaKATPα1) or Ahi1 antibodies) or 5% BSA (for anti-MHC type 1 (MHC1) or anti-MHC type 2A (MHC2A) antibodies) for 1 h at RT. Slides were then incubated with primary antibody (mouse anti-MHC1 (1:50; DSHB, BA-D5), mouse anti-MHC2A (1:50; DSHB, SC-71), mouse anti-NaKATPα1 (1:10; DSHB, a6F), or rabbit anti-Ahi1 (1:500; previously generated (Doering et al., 2008)) diluted in BSA blocking buffer overnight at 4°C. Slides were then rinsed 3 × 10 min in PBS-Tx (0.1%), followed by a 1 h incubation in secondary antibodies (1:500 - Invitrogen, A11035, goat anti-rabbit IgG AlexaFluor 546; 1:500 - Invitrogen, A11030, goat anti-mouse IgG AlexaFluor 546; 1:500 - Invitrogen, A11001, goat anti-mouse IgG Alexa Fluor 488; or 1:250 - Jackson ImmunoResearch, 715-495-151, donkey anti-mouse IgG DyLight 649, the last of which was pseudocolored in green for MHC2A images for easier visualization) diluted in BSA blocking solution. Sections

undergoing processing with two primary antibodies raised in the same species were rinsed extensively (3 × 1 h) in PBS-Tx (0.1%) prior to overnight staining with a second primary antibody. Upon completion of secondary antibody incubation, slides were stained with Hoechst 33258 (1μg/ml) in PBS for 10 min, followed by two PBS rinses and mounting of coverslips with Fluoromount G.

Muscle histology quantification

Fiber cross sectional area (CSA) was determined by measurement with NIH ImageJ software, with any muscle fibers showing evidence of damage being excluded from analysis. Myonuclear domain (MND) was quantified as total cross sectional area (μm^2) divided by total number of nuclei present.

Statistics

All statistical comparisons were performed using Statistica software. Live birth rate comparisons were performed using a Chi-square test with Bonferroni correction. Survival curves were evaluated using a Kaplan-Meier estimator with Bonferroni correction. Individual comparisons were performed using Student's t-test, while multifactorial comparisons were performed using either repeated measures ANOVA or two-way ANOVA with Bonferroni correction. Specific details regarding statistical comparisons performed on individual experiments are noted in the figure legends. All data are presented as mean ± standard error of mean (SEM).

Results

Reduced survival and growth rates in *Ahi1*$^{-/-}$ mice

To identify any lethality associated with loss of *Ahi1* and when it occurs, litters resulting from the breeding of *Ahi1*$^{+/-}$ mice were genotyped for comparison to expected Mendelian ratios. A total of 301 mice from 33 litters were analyzed, with deviations from expected live birth rates found in both *Ahi1*$^{+/-}$ and *Ahi1*$^{-/-}$ mice (Fig. 1A), indicating embryonic lethality in both *Ahi1* heterozygote ($P<0.05$) and homozygote nulls ($P<0.01$). While *Ahi1*$^{+/-}$ pups showed no increase in neonatal lethality compared to *Ahi1*$^{+/+}$ pups, *Ahi1*$^{-/-}$ pups experienced high rates of neonatal lethality ($P<0.05$). Specifically, over 40% of *Ahi1*$^{-/-}$ pups born, died prior to postnatal day (PD) 2, with over 70% dying prior to PD10 (Fig. 1B). Those surviving at PD10 showed no increased lethality and continued to survive into adulthood.

To investigate what role, if any, competition with littermates for milk contributed to neonatal lethality, litters were culled to 6 pups at PD0.5, and survival of *Ahi1*$^{-/-}$ pups was compared to that observed in litters of 10 or more pups. Reduction of litter size resulted in increased survival of *Ahi1*$^{-/-}$ pups ($P<0.05$), with ~36.8% surviving at PD21 in culled litters, with no *Ahi1*$^{-/-}$ pups surviving until the same age in large litters. Interestingly, survival rates of *Ahi1*$^{-/-}$ pups were similar through PD4 regardless of litter size, with all deviation in survival rates occurring between PD4 and PD8 (Fig. 1C), suggesting a separate mechanism is likely responsible for lethality prior to PD4.

Additionally, *Ahi1*$^{-/-}$ pups differed from *Ahi1*$^{+/+}$ littermates in body weight (P<0.001). While no differences were present at birth, by PD4.5 *Ahi1*$^{-/-}$ pups showed a ~30% reduction in body weight, a divergence which continued to increase, with PD7.5 *Ahi1*$^{-/-}$ pups having a ~50% reduction in body weight (Fig. 1D). This discrepancy in body weight persisted in surviving *Ahi1*$^{-/-}$ mice, with the most extreme reduction observed at weaning age (PD21), at which point *Ahi1*$^{-/-}$ males and females show 67.6% and 64.3% reductions in body weight, respectively, to sex-matched *Ahi1*$^{+/+}$ controls (Fig. 1E, 1F). Although body weight discrepancies decreased during adulthood in both sexes, adult male and female *Ahi1*$^{-/-}$ mice still showed body weight reductions of 37.2% and 40.2%, respectively (P<0.001).

Deficits in motor function in *Ahi1*$^{-/-}$ mice

Ahi1$^{-/-}$ mice showed deficits in various forms of motor function. When placed within a locomotor monitoring chamber for 24 h, following an acclimation period, young adult *Ahi1*$^{-/-}$ mice had drastic reductions in spontaneous locomotor activity. Specifically, compared to sex-matched controls, male *Ahi1*$^{-/-}$ mice showed a 71.5% reduction in distance travelled (P<0.01), while female *Ahi1*$^{-/-}$ mice had an 83.7% reduction (P<0.001). Moreover, while *Ahi1*$^{+/+}$ female mice travelled more than twice the distance of male *Ahi1*$^{+/+}$ mice (P<0.01), no difference was observed in the distance travelled between male and female *Ahi1*$^{-/-}$ mice (Fig. 2A).

To determine if these reductions in locomotor activity were due to a lack of motivation to explore a novel environment in *Ahi1*$^{-/-}$ mice, the initial 3 h period of acclimation on Day 0 was compared to the same 3 h period 24 h later. While *Ahi1*$^{-/-}$ mice showed reduced locomotor activity relative to sex-matched wildtype controls at every time period tested, male *Ahi1*$^{-/-}$ mice exhibited over a 15-fold increase in distance traveled during the acclimation period as compared to the experimental period (P<0.001) (~86 meters vs. ~5 meters, respectively), with female *Ahi1*$^{-/-}$ mice exhibiting over a 25-fold increase in distance traveled during the acclimation period (~102 meters vs ~3 meters) (P<0.01), indicating that the loss of locomotor activity in *Ahi1*$^{-/-}$ mice was not due to failure to recognize and explore a novel environment. While *Ahi1*$^{+/+}$ mice also showed increased locomotor activity during the acclimation period as compared to the same period the following day, the effect was less dramatic as that seen in *Ahi1*$^{-/-}$ mice, with male and female *Ahi1*$^{+/+}$ mice exhibiting 10-fold (~200 meters vs. ~17 meters) (P<0.001) and 6-fold (~234 vs. ~31 meters) (P<0.01) increases, respectively (Fig. 2B). Furthermore, we found no difference in percentage of total movement during the dark cycle, indicating no evidence of altered circadian rhythm contributing to the reduced locomotion (Fig. 2C).

In addition to reduced locomotion, we sought to identify deficits in muscle strength and function. Utilizing the suspended weights test to assess the grip strength of *Ahi1*$^{-/-}$ mice, we found decreased ability to maintain a grasp on an object in both males and females, consistently occurring from ages 4 to 9 weeks (P<0.001) (Fig. 2D, 2E).

As only a small fraction of *Ahi1*$^{-/-}$ mice survive into adulthood, we examined motor function in *Ahi1*$^{-/-}$ pups to reduce any effect of survivorship bias. To do so, we used the surface righting reflex assay to test the ability of pups at PD5.5 and PD8.5 to reorient

themselves when placed in a supine position. At both time points, *Ahi1*$^{-/-}$ pups required more time than *Ahi1*$^{+/+}$ pups to successfully roll over and remain poised on all four paws ($P<0.05$ for PD5.5; $P<0.001$ for PD8.5) (Fig. 2F). While both *Ahi1*$^{+/+}$ and *Ahi1*$^{-/-}$ pups immediately reacted to being placed upon their backs and attempting to right themselves by rolling over, the cause of the observed righting delay in *Ahi1*$^{-/-}$ pups was the inability to effectively maneuver their limbs beneath their torso.

No effect on gross brain morphology in *Ahi1*$^{-/-}$ mice

Due to known abnormal gross cerebellar morphology, which frequently occurs in humans with *AHI1* mutations (Chafai-Elalaoui et al., 2015; Ferland et al., 2004; Salva et al., 2016; Valente et al., 2006), as well as previously reported reductions in brain and cerebellar size in *Ahi1*$^{-/-}$ mice bred on a 129/SvJ/C57BL/6 genetic background (Lancaster et al., 2011), we performed analyses of total brain and cerebellar size in our *Ahi1*$^{-/-}$ mice. No gross anomalies in brain morphology were identified in 10-week old male *Ahi1*$^{-/-}$ mice on midsagittal sections (Fig. 3A, 3B), nor were any gross malformations of the cerebellum visible in transverse sections at PD21 (Fig. 3C, 3E) or 10 weeks ((Lancaster et al., 2011) Fig. 3D, 3F). Total midsagittal brain area did not differ between *Ahi1*$^{-/-}$ mice and *Ahi1*$^{+/+}$ controls at 10 weeks (Fig. 3G). Moreover, brain to total body weight ratio was ~39.1% higher in 10-week old male *Ahi1*$^{-/-}$ mice ($P<0.05$) (Fig. 3H), confirming that the loss of Ahi1 in FVB/NJ mice does not lead to decreased brain size, in contrast to the overall reductions in body size seen in *Ahi1*$^{-/-}$ mice. Indeed, although the body size of *Ahi1*$^{-/-}$ mice exhibited its most drastic discrepancy at PD21 (Fig. 1E, 1F), this same time point showed a brain to body weight ratio in *Ahi1*$^{-/-}$ mice that was more than 235% of that seen in *Ahi1*$^{+/+}$ mice ($P<0.01$) (Fig. 3H, Table 1), further indicating that brain development was not delayed in the same manner as muscle development in *Ahi1*$^{-/-}$ mice. Furthermore, neither midsagittal cerebellar area, nor the ratio of cerebellar area to total brain area were decreased in 10-week old *Ahi1*$^{-/-}$ mice (Fig. 3I, 3J).

While defective decussation of the SCPs is another hallmark of JBTS in humans, and is a component of the molar tooth sign, our FVB/NJ *Ahi1*$^{-/-}$ mice showed intact SCP decussation (Fig. 3K, 3L). To date, no reports have been published on SCP morphology in any other strain of *Ahi1*$^{-/-}$ mice, making comparisons between strains difficult. Finally, the dentate nuclei, which have been reported to be affected in humans with JBTS (Yachnis and Rorke, 1999a, b), appear unaffected in the FVB/NJ *Ahi1*$^{-/-}$ mouse (Fig. 3C, 3E).

Embryonic muscle tissue from *Ahi1*$^{-/-}$ mice shows defects in desmin expression

To identify a role for Ahi1 in the proper development of hindlimb muscle tissue, hindlimbs were removed from ED18.5 *Ahi1*$^{+/+}$ and *Ahi1*$^{-/-}$ embryos for cryosectioning and immunolabeling of Ahi1 in developing muscle tissue. While transverse sections of hindlimbs from *Ahi1*$^{+/+}$ embryos contain Ahi1-positive cells within the developing musculature (Fig. 4A), no such Ahi1-positive structures are present in the hindlimbs of *Ahi1*$^{-/-}$ embryos (Fig. 4B).

Importantly, *Ahi1*$^{-/-}$ ED18.5 embryos also show evidence of a muscle-specific defect compared to wildtype embryos in reduced levels of desmin, a ~53 kDa muscle-specific type

III intermediate filament (Hnia et al., 2015)(Fig. 4C, 4D). While a known degradation product of desmin (Baron et al., 2004) is visible as a ~46 kDa band (Fig. 4C), total desmin levels including this degradation product are also reduced in *Ahi1*$^{-/-}$ embryos compared to *Ahi1*$^{+/+}$ controls (Fig. 4E). Interestingly, despite reductions in both 53 kDa desmin and total desmin expression, embryonic *Ahi1*$^{-/-}$ muscle tissue displays a higher amount of degradation product (< 53 kDa) relative to total desmin levels (Fig. 4F), suggesting potential dysregulation of the degradation of desmin by proteolytic enzymes that occurs during myoblast differentiation (Elamrani et al., 1995), and is ongoing at ED18.5 (Yamane, 2005).

Ahi1$^{-/-}$ primary myoblasts showed deficits in differentiation but not proliferation *in vitro*

To identify the effect of the loss of *Ahi1* on myoblasts that might explain the motor deficits observed in these mice, we cultured primary myoblasts from PD1.5 mice to analyze how proliferation and differentiation were affected. After harvesting and purification to remove fibroblasts, myoblasts were allowed to proliferate for 2 d in PM, prior to comparison of proliferation rates in PM and 1 d in DM (a low serum condition known to induce myoblasts to differentiate), using 4 h BrdU incorporation as a marker for cell proliferation. Primary myoblasts from both *Ahi1*$^{+/+}$ and *Ahi1*$^{-/-}$ pups showed similar proliferation rates during growth in PM, as well as the expected reduction of proliferation rates during exposure to DM, indicating that no proliferation deficits occur in myoblasts from *Ahi1*$^{-/-}$ mice (Fig. 5A).

Primary myoblasts from *Ahi1*$^{+/+}$ and *Ahi1*$^{-/-}$ pups were then subjected to 3 d in DM and muscle heavy chain (MHC) protein expression was assessed as a marker of differentiation (Fu et al., 2014). As expected, no differences were found in cells not yet exposed to differentiation conditions (Day 0). However, myoblasts from *Ahi1*$^{+/+}$ pups showed more than a 3-fold increase in normalized MHC expression after 3 d (P<0.01) in DM, whereas no such increase was found in myoblasts from *Ahi1*$^{-/-}$ pups (P<0.001 Day 3 *Ahi1*$^{+/+}$ vs. *Ahi1*$^{-/-}$) (Fig. 5B, 5C).

Reductions in hindlimb muscle mass, fiber CSA and myonuclear domain *in vivo*

We next attempted to identify evidence of deficits in skeletal muscle development in tissue from *Ahi1*$^{-/-}$ mice. Gross morphological analysis of hindlimbs from PD21 male *Ahi1*$^{-/-}$ mice showed a dramatic reduction in muscle tissue compared to age- and sex-matched *Ahi1*$^{+/+}$ mice (Fig. 6A, 6B). In contrast to increases in brain to total body mass ratios at 3 weeks (Fig. 3H, Table 1), absolute mass of gastrocnemius, soleus, and quadriceps muscles were reduced ~70.6% (P<0.001), ~76.9% (P<0.05), and ~65.5% (P<0.01), respectively, in male *Ahi1*$^{-/-}$ mice (Table 1). Muscle fiber cross section analysis of rectus femoris (RF) in PD21 male *Ahi1*$^{+/+}$ (Fig. 6C) and *Ahi1*$^{-/-}$ (Fig. 6D) mice revealed fiber CSA reductions of ~68.9% (P<0.01) (Fig. 6E), as well as a reduction in total RF to femur cross sectional area ratio (3.5 ± 0.4 in *Ahi1*$^{+/+}$ mice vs. 2.4 ± 0.1 in *Ahi1*$^{-/-}$ mice, P<0.05). Furthermore, as PD21 is reported to be the developmental time point at which mouse muscle tissue ceases to add new nuclei (White et al., 2010), we quantified the number of nuclei in cross sections of RF, finding a decrease of nuclei per myofiber of ~46.6% in *Ahi1*$^{-/-}$ mice (P<0.01) (Fig. 6F). To account for overall reductions in muscle mass, we then examined myonuclear domain, calculated as area in μm^2 per nuclei in cross section, identifying a reduction of ~40.4% in

Ahi1$^{-/-}$ RF (P<0.05) (Fig. 6G), suggesting that each nucleus in *Ahi1*$^{-/-}$ muscle supports a reduced area of tissue as compared to nuclei in *Ahi1*$^{+/+}$ mice.

Next, to further examine the reduction of CSA in specific muscle fiber types, we utilized antibodies for MHC type 1 (MHC1) and MHC type 2A (MHC2A) to compare muscle fiber CSA in soleus (Fig. 7A, 7C) and vastus intermedius (VI) muscles (Fig. 7B, 7D), two muscles which express a mixture of fiber types. In both muscles, both fiber types analyzed had reduced fiber CSA in *Ahi1*$^{-/-}$ mice. Specifically, soleus fiber CSA was reduced ~46.4% for MHC1 fibers (P<0.05), and ~53.9% for MHC2A fibers (P<0.01) (Fig. 7E). Within the VI, MHC1 fiber CSA was reduced by ~47.5% (P<0.01), while MHC2A fiber CSA was reduced by ~62.8% (P<0.01) (Fig. 7F). Moreover, the distribution of individual muscle fiber CSA within each muscle and muscle fiber type showed minimal overlap between genotypes, with the overall range of CSAs being reduced in *Ahi1*$^{-/-}$ mice (Fig. 7G–J).

As body size discrepancies seen at 3 weeks are reduced in adult mice (Fig. 1E–1F), we sought to determine if reductions in fiber CSA identified at 3 weeks would persist into adulthood in soleus and VI muscles (Fig. 8A–D). While the differences in CSA in muscle fibers of MHC1 and MHC2A were reduced in both muscles analyzed in 3-month old *Ahi1*$^{-/-}$ mice than those seen at 3 weeks, the size of the effect witnessed at 3 months was muscle dependent. Specifically, within the soleus, CSA of MHC1 and MHC2A fibers were significantly reduced in *Ahi1*$^{-/-}$ mice by ~22.6% (P<0.05) and ~14.7% (P<0.05), respectively (Fig. 8E), showing a lessened effect than that observed at 3 weeks. Interestingly, the CSA of both fiber types in the VI did not show a significant decrease to those in *Ahi1*$^{+/+}$ mice at 3 months (Fig. 8F), indicating a delayed maturation, rather than a persistent reduction.

Discussion

Here, we have identified evidence of deficits in several measures of motor function in *Ahi1*$^{-/-}$ mice, beginning with delays in motor development observable in early development, with deficits of motor and muscle function persisting into adulthood in the small percentage of *Ahi1*$^{-/-}$ mice that survive. While humans with JBTS exhibit similar delays and difficulties with motor function, including hypotonia and eventual ataxia (Parisi and Glass, 1993 [updated 2017]; Parisi et al., 2007; Romani et al., 2013), our *Ahi1*$^{-/-}$ mice show no evidence of gross neuroanatomical malformations (or ataxia) commonly seen in humans with JBTS, including aplasia/hypoplasia of the cerebellar vermis, to which the accompanying motor deficits are frequently attributed.

Indeed, brain to body weight ratios at 3 and 10 weeks of age show that gross brain development precedes body development in *Ahi1*$^{-/-}$ mice. Importantly, we found that Ahi1 is expressed in developing muscle in *Ahi1*$^{+/+}$ embryos (and as expected not in *Ahi1*$^{-/-}$ embryos). Moreover, we show histological evidence of underdeveloped muscle tissue in *Ahi1*$^{-/-}$ mice at weaning age, which is attenuated partially or completely by three months of age, with the extent of the recovery varying between muscles. However, a deficit in desmin expression is present in ED18.5 *Ahi1*$^{-/-}$ embryo muscle, suggesting a defect specific to developing muscle. Furthermore, we find that isolated primary myoblasts from *Ahi1*$^{-/-}$ mice

show deficits in differentiation when exposed to appropriate conditions *in vitro* with no changes in proliferation. Overall, these results suggest that Ahi1 plays a role in myoblast differentiation, which would account for the deficits in muscle development observed in *Ahi1*$^{-/-}$ mice.

While the symptoms of JBTS show considerable heterogeneity and often affect multiple organ systems, those affecting the development of motor function are among the most frequently reported, and are considered a key component of the symptomology (Parisi and Glass, 1993 [updated 2017]; Parisi et al., 2007; Romani et al., 2013). Notably, children with JBTS show delays in developmental milestones, including an average age of ~11 months upon first rolling over (as compared to a typical age of ~5 months), and an average age of ~4 years to begin walking independently (as compared to a typical age of ~12 months), with some individuals never reaching the latter milestone (Gerber et al., 2010; Steinlin et al., 1997). Using the surface righting reflex assay in *Ahi1*$^{-/-}$ neonatal mice, we have observed a similar delay in the ability to rapidly reorient when placed upon their backs, which improves over time but trails the performance of *Ahi1*$^{+/+}$ mice developmentally. Similarly, the ability to maintain a grip on increasing weights is both delayed and reduced in *Ahi1*$^{-/-}$ mice from weaning age through 9 weeks, and reduced locomotor activity is seen in early adulthood (that is not the result of decreased exploratory interest).

Although motor symptoms are common in those with JBTS, the presence of some level of neuroanatomical malformation within these individuals makes it difficult, if not impossible, to separate the two. Here, the finding that *Ahi1*$^{-/-}$ mice on an FVB/NJ background do not display the gross neuroanatomical malformations seen in humans with JBTS, but do show deficits in motor function, suggests that there may be a component of these symptoms which is independent of the CNS. Furthermore, the presence of reductions in cerebellar development previously reported in 129/SvJ/C57Bl/6J *Ahi1*$^{-/-}$ mice (Lancaster et al., 2011) indicates that various aspects of the loss of Ahi1 in mice are strain specific, allowing for the opportunity to further separate independent phenotypic features. In addition to neuroanatomical differences between strains, global *Ahi1*$^{-/-}$ mice on a mixed 129vEV/C57BL/6N genetic background show reductions in spontaneous locomotor activity and body weight during development, although each appears to have reduced severity in comparison to our global FVB/NJ *Ahi1*$^{-/-}$ mice, with those on a mixed background reaching equivalent body weight to *Ahi1*$^{+/+}$ controls by PD26 (Weng et al., 2013). However, the most telling comparisons between *Ahi1*$^{-/-}$ mice may be those involving differences between the loss of *Ahi1* globally versus conditionally. Specifically, conditional *Ahi1*$^{fl/fl}$ mice utilizing the neuronal nestin promoter to drive Cre recombinase knockout of floxed *Ahi1* show no reductions in locomotor activity, body weight, or perinatal survival, all of which are reported in global *Ahi1*$^{-/-}$ mice generated within the same laboratories (Louie et al., 2010; Weng et al., 2013; Xu et al., 2010). These data, viewed collectively, suggest that while neuroanatomical malformations due to the loss of Ahi1 may vary between strains, motor function, body development, and lethality are due to the impact on body systems outside of the CNS. Admittedly, the discrepancies observed in neuroanatomical development between *Ahi1*$^{-/-}$ mice on an FVB/NJ genetic background as compared to those reported on other mouse strains and humans with JBTS suggest that this model may not be ideal for the study of *Ahi1* in neurodevelopment. At the same time, the presence of motor function deficits in

both humans with JBTS and in FVB/NJ *Ahi1*$^{-/-}$ mice make this strain particularly useful when investigating motor and muscle deficits, as it eliminates the confounding factor of neurological influence on muscle development and function.

While the impact of causative mutations of JBTS on the development of the muscular system has not been given proper attention, *AHI1*/*Ahi1* mRNA has been found to be expressed in human and rodent skeletal muscle tissue, as well as in rat primary myoblasts (Prior et al., 2010). Additionally, microRNA (miRNA) silencing of *centrosomal protein of 290* kDa (*Cep290*), another gene implicated in JBTS, has been shown to decrease the *in vitro* differentiation potential of immortalized C2C12 mouse myoblasts (Fu et al., 2014). While *AHI1* and *CEP290* are only two of over 30 known genes in which mutations are known to cause JBTS, together they are estimated to be responsible for ~14–27% of known cases (Romani et al., 2013). While the neuroanatomical malformations seen in humans with JBTS would be expected to contribute heavily to motor and muscular symptoms, *in vitro* data linking improper differentiation to two of the more common genes implicated in JBTS further suggests that the possibility of muscle-specific effects on development warrant further consideration. In fact, such deficits could potentially underlie the symptomology seen in JBTS as a result of various other mutations. Additionally, the presence of a desmin defect at ED18.5 in *Ahi1*$^{-/-}$ mice further suggests the likelihood of a muscle-specific pathology. The ~46 kDa desmin degradation product found in relatively higher levels (as a ratio to 53 kDa desmin) in *Ahi1*$^{-/-}$ embryos has been shown to be a product of desmin cleavage by proteolytic calpain enzymes (Baron et al., 2004), which are essential to muscle differentiation (Barnoy et al., 1998). Thus, one possibility, which should be further investigated, is whether Ahi1 may play a role in regulating levels of various calpain enzymes, as well as levels of the endogenous calpain inhibitor, calpastatin. As the levels of calpain and calpastatin typically fluctuate in a tightly regulated manner during the differentiation process (Barnoy et al., 1996; Dourdin et al., 1999), the loss of a protein, which is involved in the regulation of calpain and calpastatin, could explain the reduced levels of desmin and excess levels of its degradation product observed in *Ahi1*$^{-/-}$ embryos.

A common feature of all known JBTS causative genes is their localization to the primary cilium or supporting structures, and/or involvement in the generation, maintenance and function of the primary cilium (Brancati et al., 2010; Romani et al., 2013). Indeed, previous studies have shown that in several cell and tissue types, Ahi1 localizes to the basal body, from which the primary cilium protrudes (Eley et al., 2008). This common feature of all genes known to be mutated in JBTS has led to the categorization of JBTS as a ciliopathy. To date, minimal research has been conducted on the role of primary cilia in skeletal muscle development. However, it is presumptive to assume that the role of proteins related to primary cilia function have no extraciliary roles in this process. Indeed, in the developing hindlimb musculature of ED18.5 FVB/NJ mice, immunolabeling of Ahi1 shows an extraciliary localization. Moreover, many so-called “cilia proteins” have been shown to have extraciliary locations and functions (Hua and Ferland, 2018a, b), leaving open the possibility that mutations known to cause JBTS may contribute to the observed symptomology at least partially through extraciliary mechanisms. Lastly, previous work in our laboratory has shown that observed subcellular localizations of cilia proteins is heavily dependent upon fixation method, including several proteins known to be causative for JBTS in humans (Hua

and Ferland, 2017), further underscoring the possibility that these proteins may have yet unknown extraciliary localization (and thus, extraciliary functions).

The impact of mutations seen in genes associated with JBTS on the development of the muscular system may be easily overlooked due to the appearance of obvious brain malformations, such as the MTS and cerebellar vermis aplasia. However, the elimination of the possibility of such a CNS-independent component may be premature, as no data are available looking specifically at muscle development in those with JBTS. While treatment for motor deficits identified in JBTS is currently limited to supportive measures (Parisi et al., 2007), the identification of a muscle specific, CNS-independent component may be amenable to the development of future therapies which seek to better manage this aspect of JBTS symptomology.

Acknowledgements

Research reported in this publication was supported, in part, by the National Institute of Neurological Disorders and Stroke of the National Institutes of Health under Award R01 NS092062. The content is solely the responsibility of the authors and does not necessarily represent the official views of the National Institutes of Health. The hybridoma, monoclonal antibodies to BrdU, myosin heavy chain (MHC), MHC1, MHC2A, and NaKATPα1 developed by S.J. Kaufman (BrdU), D.A. Fischman (Desmin and MHC), S. Schiaffino (MHC1 and MHC2A), and D.M. Fambrough (NaKATPα1) were obtained from the Developmental Studies Hybridoma Bank, created by the NICHD of the NIH and maintained at The University of Iowa, Department of Biology, Iowa City, IA 52242.

ABBREVIATIONS

AHI1	Abelson helper integration site 1
BrdU	5-bromo-2’-deoxyuridine
CNS	Central nervous system
CSA	Cross sectional area
DM	Differentiation medium
DSHB	Developmental studies hybridoma bank
MHC	Myosin heavy chain
JBTS	Joubert syndrome
PM	Proliferation medium
RF	Rectus femoris
SCP	Superior cerebellar peduncles
VI	Vastus intermedius

References

Barnoy S, Glaser T, Kosower NS, 1998 The calpain-calpastatin system and protein degradation in fusing myoblasts. Biochim Biophys Acta 1402, 52–60. [PubMed: 9551085]

Barnoy S, Glasner T, Kosower NS, 1996 The role of calpastatin (the specific calpain inhibitor) in myoblast differentiation and fusion. Biochem Biophys Res Commun 220, 933–938. [PubMed: 8607870]

Baron CP, Jacobsen S, Purslow PP, 2004 Cleavage of desmin by cysteine proteases: Calpains and cathepsin B. Meat Sci 68, 447–456. [PubMed: 22062413]

Brancati F, Dallapiccola B, Valente EM, 2010 Joubert Syndrome and related disorders. Orphanet J Rare Dis 5, 20. [PubMed: 20615230]

Chafai-Elalaoui S, Chalon M, Elkhartoufi N, Kriouele Y, Mansouri M, Attie-Bitach T, Sefiani A, Baala L, 2015 A homozygous AHI1 gene mutation (p.Thr304AsnfsX6) in a consanguineous Moroccan family with Joubert syndrome: a case report. J Med Case Rep 9, 254. [PubMed: 26541515]

Deacon RM, 2013 Measuring the strength of mice. J Vis Exp 76.

Dempsey JC, Phelps IG, Bachmann-Gagescu R, Glass IA, Tully HM, Doherty D, 2017 Mortality in Joubert syndrome. Am J Med Genet A 173, 1237–1242. [PubMed: 28371402]

Dixon-Salazar T, Silhavy JL, Marsh SE, Louie CM, Scott LC, Gururaj A, Al-Gazali L, Al-Tawari AA, Kayserili H, Sztriha L, Gleeson JG Mutations in the AHI1 gene, encoding Jouberin, cause Joubert syndrome with cortical polymicrogyria. Am. J. Hum. Genet 75, 2004, 979–987. [PubMed: 15467982]

Doering JE, Kane K, Hsiao YC, Yao C, Shi B, Slowik AD, Dhagat B, Scott DD, Ault JG, Page-McCaw PS, Ferland RJ, 2008 Species differences in the expression of Ahi1, a protein implicated in the neurodevelopmental disorder Joubert syndrome, with preferential accumulation to stigmoid bodies. J Comp Neurol 511, 238–256. [PubMed: 18785627]

Dourdin N, Balcerzak D, Brustis JJ, Poussard S, Cottin P, Ducastaing A, 1999 Potential m-calpain substrates during myoblast fusion. Exp Cell Res 246, 433–442. [PubMed: 9925759]

Edvardson S, Shaag A, Zenvirt S, Erlich Y, Hannon GJ, Shanske AL, Gomori JM, Ekstein J, Elpeleg O, 2010 Joubert syndrome 2 (JBTS2) in Ashkenazi Jews is associated with a TMEM216 mutation. Am J Hum Genet 86, 93–97. [PubMed: 20036350]

Elamrani N, Brustis JJ, Dourdin N, Balcerzak D, Poussard S, Cottin P, Ducastaing A, 1995 Desmin degradation and Ca(2+)-dependent proteolysis during myoblast fusion. Biol Cell 85, 177–183. [PubMed: 8785519]

Eley L, Gabrielides C, Adams M, Johnson CA, Hildebrandt F, Sayer JA, 2008 Jouberin localizes to collecting ducts and interacts with nephrocystin-1. Kidney Int 74, 1139–1149. [PubMed: 18633336]

Ferland RJ, Eyaid W, Collura RV, Tully LD, Hill RS, Al-Nouri D, Al-Rumayyan A, Topcu M, Gascon G, Bodell A, Shugart YY, Ruvolo M, Walsh CA, 2004 Abnormal cerebellar development and axonal decussation due to mutations in AHI1 in Joubert syndrome. Nat Genet 36, 1008–1013. [PubMed: 15322546]

Fu W, Asp P, Canter B, Dynlacht BD, 2014 Primary cilia control hedgehog signaling during muscle differentiation and are deregulated in rhabdomyosarcoma. Proc Natl Acad Sci U S A 111, 9151–9156. [PubMed: 24927541]

Gerber RJ, Wilks T, Erdie-Lalena C, 2010 Developmental milestones: motor development. Pediatr Rev 31, 267–276. [PubMed: 20595440]

Hnia K, Ramspacher C, Vermot J, Laporte J, 2015 Desmin in muscle and associated diseases: beyond the structural function. Cell Tissue Res 360, 591–608. [PubMed: 25358400]

Hsiao YC, Tong ZJ, Westfall JE, Ault JG, Page-McCaw PS, Ferland RJ, 2009 Ahi1, whose human ortholog is mutated in Joubert syndrome, is required for Rab8a localization, ciliogenesis and vesicle trafficking. Hum Mol Genet 18, 3926–3941. [PubMed: 19625297]

Hua K, Ferland RJ, 2017 Fixation methods can differentially affect ciliary protein immunolabeling. Cilia 6, 5. [PubMed: 28352462]

Hua K, Ferland RJ, 2018a Primary cilia proteins: ciliary and extraciliary sites and functions. Cell Mol Life Sci 75, 1521–1540. [PubMed: 29305615]

Hua K, Ferland RJ, 2018b Primary Cilia Reconsidered in the Context of Ciliopathies: Extraciliary and Ciliary Functions of Cilia Proteins Converge on a Polarity theme? Bioessays 40, e1700132. [PubMed: 29882973]

Koshy B, Oommen SP, Jasper S, Danda S, Surendrababu NR, 2010 Development and dysmorphism in Joubert syndrome--short case series from India. J Trop Pediatr 56, 209–212. [PubMed: 19755534]

Lancaster MA, Gopal DJ, Kim J, Saleem SN, Silhavy JL, Louie CM, Thacker BE, Williams Y, Zaki MS, Gleeson JG, 2011 Defective Wnt-dependent cerebellar midline fusion in a mouse model of Joubert syndrome. Nat Med 17, 726–731. [PubMed: 21623382]

Louie CM, Caridi G, Lopes VS, Brancati F, Kispert A, Lancaster MA, Schlossman AM, Otto EA, Leitges M, Grone HJ, Lopez I, Gudiseva HV, O'Toole JF, Vallespin E, Ayyagari R, Ayuso C, Cremers FP, den Hollander AI, Koenekoop RK, Dallapiccola B, Ghiggeri GM, Hildebrandt F, Valente EM, Williams DS, Gleeson JG, 2010 AHI1 is required for photoreceptor outer segment development and is a modifier for retinal degeneration in nephronophthisis. Nat Genet 42, 175–180. [PubMed: 20081859]

Maria BL, Hoang KB, Tusa RJ, Mancuso AA, Hamed LM, Quisling RG, Hove MT, Fennell EB, Booth-Jones M, Ringdahl DM, Yachnis AT, Creel G, Frerking B, 1997 "Joubert syndrome" revisited: key ocular motor signs with magnetic resonance imaging correlation. J Child Neurol 12, 423–430. [PubMed: 9373798]

Parisi M, Glass I, 1993 [updated 2017]. Joubert Syndrome, in: Adam MP, Ardinger HH, Pagon RA, Wallace SE, Bean LJH, Stephens K, Amemiya A (Eds.), GeneReviews((R)), Seattle (WA).

Parisi MA, Doherty D, Chance PF, Glass IA, 2007 Joubert syndrome (and related disorders) (OMIM 213300). Eur J Hum Genet 15, 511–521. [PubMed: 17377524]

Prior MJ, Foletta VC, Jowett JB, Segal DH, Carless MA, Curran JE, Dyer TD, Moses EK, McAinch AJ, Konstantopoulos N, Bozaoglu K, Collier GR, Cameron-Smith D, Blangero J, Walder KR, 2010 The characterization of Abelson helper integration site-1 in skeletal muscle and its links to the metabolic syndrome. Metabolism 59, 1057–1064. [PubMed: 20045148]

Romani M, Micalizzi A, Valente EM, 2013 Joubert syndrome: congenital cerebellar ataxia with the molar tooth. Lancet Neurol 12, 894–905. [PubMed: 23870701]

Salva I, Albuquerque C, Moreira A, Damaso C, 2016. Nystagmus in a newborn: a manifestation of Joubert syndrome in the neonatal period. BMJ Case Rep 2016.

Steinlin M, Schmid M, Landau K, Boltshauser E, 1997 Follow-up in children with Joubert syndrome. Neuropediatrics 28, 204–211. [PubMed: 9309710]

Strongin A, Heller T, Doherty D, Glass IA, Parisi MA, Bryant J, Choyke P, Turkbey B, Daryanani K, Yildirimli D, Vemulapalli M, Mullikin JC, Malicdan MC, Vilboux T, Gahl WA, Gunay-Aygun M, Program NCS, 2018 Characteristics of Liver Disease in 100 Individuals With Joubert Syndrome Prospectively Evaluated at a Single Center. J Pediatr Gastroenterol Nutr 66, 428–435. [PubMed: 29112083]

Tunovic S, Baranano KW, Barkovich JA, Strober JB, Jamal L, Slavotinek AM, 2015 Novel KIF7 missense substitutions in two patients presenting with multiple malformations and features of acrocallosal syndrome. Am J Med Genet A 167A, 2767–2776. [PubMed: 26174511]

Valente EM, Brancati F, Silhavy JL, Castori M, Marsh SE, Barrano G, Bertini E, Boltshauser E, Zaki MS, Abdel-Aleem A, Abdel-Salam GM, Bellacchio E, Battini R, Cruse RP, Dobyns WB, Krishnamoorthy KS, Lagier-Tourenne C, Magee A, Pascual-Castroviejo I, Salpietro CD, Sarco D, Dallapiccola B, Gleeson JG, International JSG, 2006 AHI1 gene mutations cause specific forms of Joubert syndrome-related disorders. Ann Neurol 59, 527–534. [PubMed: 16453322]

Weiss AH, Doherty D, Parisi M, Shaw D, Glass I, Phillips JO, 2009 Eye movement abnormalities in Joubert syndrome. Invest Ophthalmol Vis Sci 50, 4669–4677. [PubMed: 19443711]

Weng L, Lin YF, Li AL, Wang CE, Yan S, Sun M, Gaertig MA, Mitha N, Kosaka J, Wakabayashi T, Xu X, Tang B, Li S, Li XJ, 2013 Loss of Ahi1 affects early development by impairing BM88/Cend1-mediated neuronal differentiation. J Neurosci 33, 8172–8184. [PubMed: 23658157]

White RB, Bierinx AS, Gnocchi VF, Zammit PS, 2010 Dynamics of muscle fibre growth during postnatal mouse development. BMC Dev Biol 10, 21. [PubMed: 20175910]

Xu X, Yang H, Lin YF, Li X, Cape A, Ressler KJ, Li S, Li XJ, 2010 Neuronal Abelson helper integration site-1 (Ahi1) deficiency in mice alters TrkB signaling with a depressive phenotype. Proc Natl Acad Sci U S A 107, 19126–19131. [PubMed: 20956301]

Yachnis AT, Rorke LB, 1999a Cerebellar and brainstem development: an overview in relation to Joubert syndrome. J Child Neurol 14, 570–573. [PubMed: 10488901]

Yachnis AT, Rorke LB, 1999b Neuropathology of Joubert syndrome. J Child Neurol 14, 655–659; [PubMed: 10511338]

Yamane A, 2005 Embryonic and postnatal development of masticatory and tongue muscles. Cell Tissue Res 322, 183–189. [PubMed: 16041600]

Highlights

- Mice with targeted deletions of *Ahi1* show deficits in motor behavior
- Primary myoblasts from *Ahi1* knockout mice fail to properly differentiate *in vitro*
- Muscle in $Ahi1^{-/-}$ mice show reduced myonuclear domain & fiber cross sectional area
- Reductions in the muscle filament, desmin, are present in embryonic $Ahi1^{-/-}$ mice
- No neuroanatomical malformations are observed in FVB/NJ $Ahi1^{-/-}$ mice

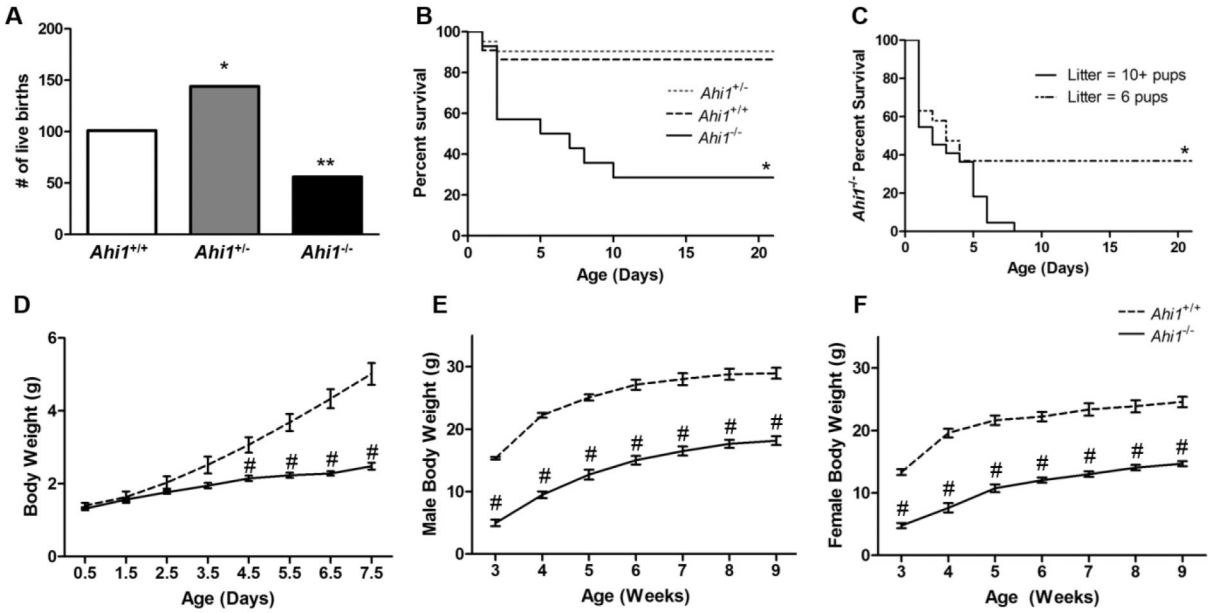

Figure 1. Embryonic and neonatal lethality, and reductions in body weight exhibited by *Ahi1*$^{-/-}$ mice.

(A) Breeding of *Ahi1*$^{+/-}$ mice resulted in non-Mendelian live birth ratios, with both *Ahi1*$^{+/-}$ and *Ahi1*$^{-/-}$ pups being born at lower frequencies than expected based on frequency of *Ahi1*$^{+/+}$ pups (* = P<0.05, ** = P<0.01, Chi-square test with Bonferroni correction; n = 301 pups from 33 litters). (B) *Ahi1*$^{-/-}$ pups show increased lethality in the early neonatal period, with the majority dying prior to PD10 (Kaplan-Meier estimator with Bonferonni correction; data from 9 litters; n = 23 *Ahi1*$^{+/+}$, 42 *Ahi1*$^{+/-}$, 15 *Ahi1*$^{-/-}$). (C) Comparison of *Ahi1*$^{-/-}$ neonate survival in litters of 10 or more pups vs. litters culled to 6 pups at PD0.5 revealing that Ahi1$^{-/-}$ pups from culled litters are more likely to survive to weaning age (Kaplan-Meyer estimator; n = 19–22 *Ahi1*$^{-/-}$ per condition). (D) *Ahi1*$^{-/-}$ pups do not differ in body weight from *Ahi1*$^{+/+}$ littermates at birth, but fail to gain weight over the neonatal period. Deficits in body weight persist into adulthood in both surviving male (E) and female (F) *Ahi1*$^{-/-}$ mice (# = P<0.001; repeated measures ANOVA; n = 5–7 per group). Data are presented as the mean ± standard error of the mean (SEM).

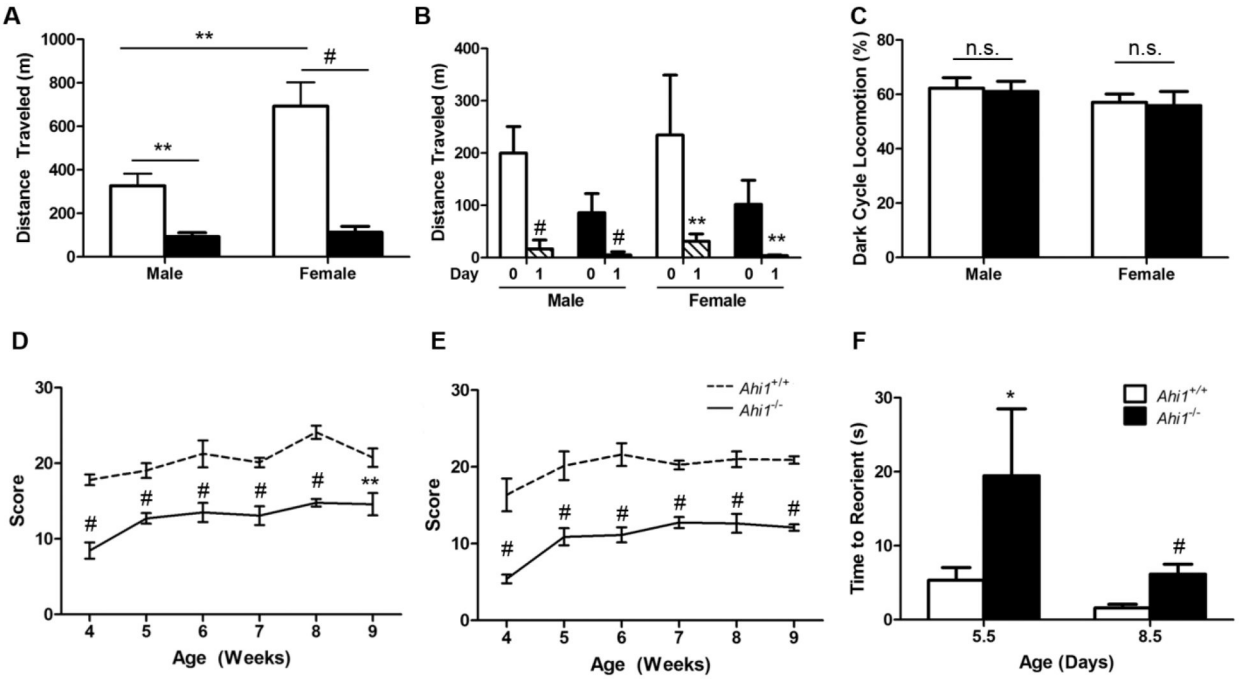

Figure 2. Reduced performance in measures of motor function.

(A) Total distance travelled in locomotion chamber over a 24 h period is reduced in both male and female 7- to 9-week old *Ahi1*$^{-/-}$ mice, compared to sex-matched controls (** = $P<0.01$, # = $P<0.001$, two-way ANOVA with Bonferroni correction; n = 6–8 per group). (B) Analysis of spontaneous locomotion during the initial 3 h acclimation period (Day 0) compared to the same period 24 h later (Day 1) reveals increased spontaneous locomotor activity during the initial acclimation period (# = $P<0.001$, paired t-test) regardless of sex or genotype. (C) Comparisons of percentage of total distance travelled during the dark cycle show no difference between *Ahi1*$^{+/+}$ and *Ahi1*$^{-/-}$ mice of either sex. Both (D) male and (E) female *Ahi1*$^{-/-}$ mice show deficits in ability to maintain a grasp on weights of increasing mass in the suspended weights test, which persist through the testing period of 4 to 9 weeks of age (repeated measures ANOVA; n = 5–7 per group). (F) Surface righting reflex assay indicates delays in motor performance were present from the earliest points examined, with 5- and 8-d old *Ahi1*$^{-/-}$ pups showing increased latency to properly reorient when placed on their backs on a hard surface (* = $P<0.05$, Student's t-test; n = 3–6 per group). Data are presented as the mean ± standard error of the mean (SEM).

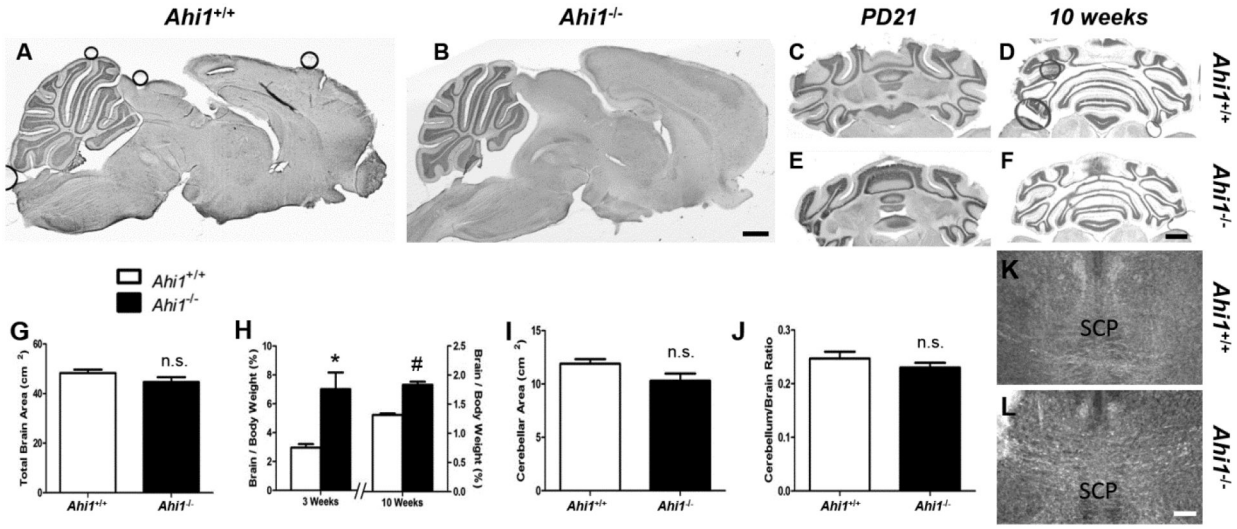

Figure 3. *Ahi1*$^{-/-}$ mice show no evidence of gross neuroanatomical malformations.

Representative cresyl violet stained midsagittal (A, B) and transverse (C–F) sections from *Ahi1*$^{+/+}$ (A, C, D) and *Ahi1*$^{-/-}$ (B, E, F) mice show no observable difference in gross morphology of total brain or cerebellar vermis in midsagittal sections at 10 weeks of age (A, B), nor evidence of gross cerebellar malformations in transverse sections at PD21 (C, E) or 10 weeks (D, F). Brain development is not delayed to the extent seen in overall body weight. Total brain area (G) and cerebellar area (I) are not reduced in midsagittal sections of 10-week old *Ahi1*$^{-/-}$ mice, nor is the ratio of cerebellum to total brain area (J). (H) Brain to total body weight ratio is higher in *Ahi1*$^{-/-}$ mice at 3 and 10 weeks, showing body development lags behind development of the brain (* = P<0.05, # = P<0.001, Student's t-test; n = 3–4 at 3 weeks, 4–5 at 10 weeks). Immunolabeling of myelin basic protein to identify white matter tracts in 10 week old transverse brain sections in *Ahi1*$^{+/+}$ (K) and *Ahi1*$^{-/-}$ (L) mice show similar SCP decussation. Data are presented as the mean ± standard error of the mean (SEM). Scale bars = 1 mm (A–F) and 200 μm (K, L)

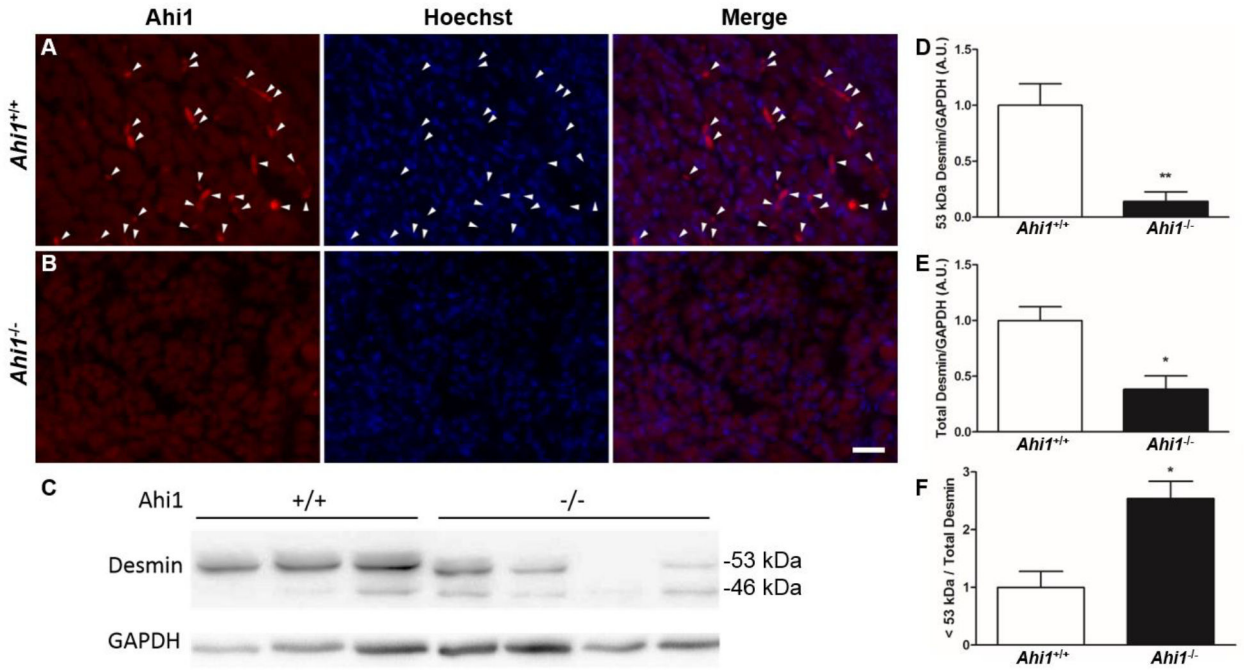

Figure 4. Evidence of muscle specific defects at ED18.5.

Ahi1-positive cells (white arrowheads) are present in the developing hindlimb muscle tissue of $Ahi1^{+/+}$ mice at ED18.5 (A), but are absent (as expected) from $Ahi1^{-/-}$ mice (B). The loss of Ahi1 leads to reduced overall desmin levels and increased desmin degradation products in ED18.5 hindlimb muscle tissue. (C) Western blot of desmin from $Ahi1^{+/+}$ and $Ahi1^{-/-}$ ED18.5 hindlimb muscle tissue showing levels of desmin at the appropriate molecular weight of 53 kDa, as well as a known degradation product at 46 kDa. Quantification of desmin indicates that $Ahi1^{-/-}$ embryos have reduced levels of 53 kDa desmin (D), as well as reductions in total levels of desmin (53 kDa plus degradation products) (E). Furthermore, hindlimb muscle tissue from $Ahi1^{-/-}$ embryos show an increased level of desmin degradation products (<53 kDa) relative to total desmin levels (F) (* = $P<0.05$, ** = $P<0.01$, Student's t-test; n = 3–4 per group). Scale bar = 25 μm.

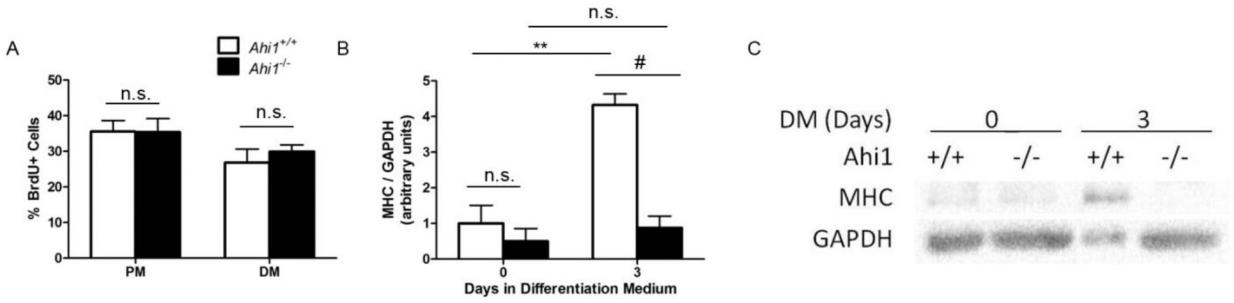

Figure 5. *In vitro* analysis of primary myoblasts.

Primary myoblasts harvested from PD1.5 $Ahi1^{+/+}$ and $Ahi1^{-/-}$ pups were labeled for incorporated BrdU in nuclei under both proliferation and early differentiation conditions. (A) Quantification of percentage of proliferating cells under each condition (n = 3 independent cell lines per condition, observed in duplicate) showing no change in proliferation between genotypes when exposed to similar conditions. (B) Quantification of MHC levels, normalized to GAPDH, of $Ahi1^{+/+}$ and $Ahi1^{-/-}$ primary myoblasts in proliferation medium and following 3 d in differentiation medium. (C) Representative western blot of data quantified in (B) (** = $P<0.01$, # = $P<0.001$, two-way ANOVA with Bonferroni correction; n = 3 independent cell lines per condition, collected in triplicate; levels normalized to $Ahi1^{+/+}$ Day 0). Data are presented as the mean ± standard error of the mean (SEM).

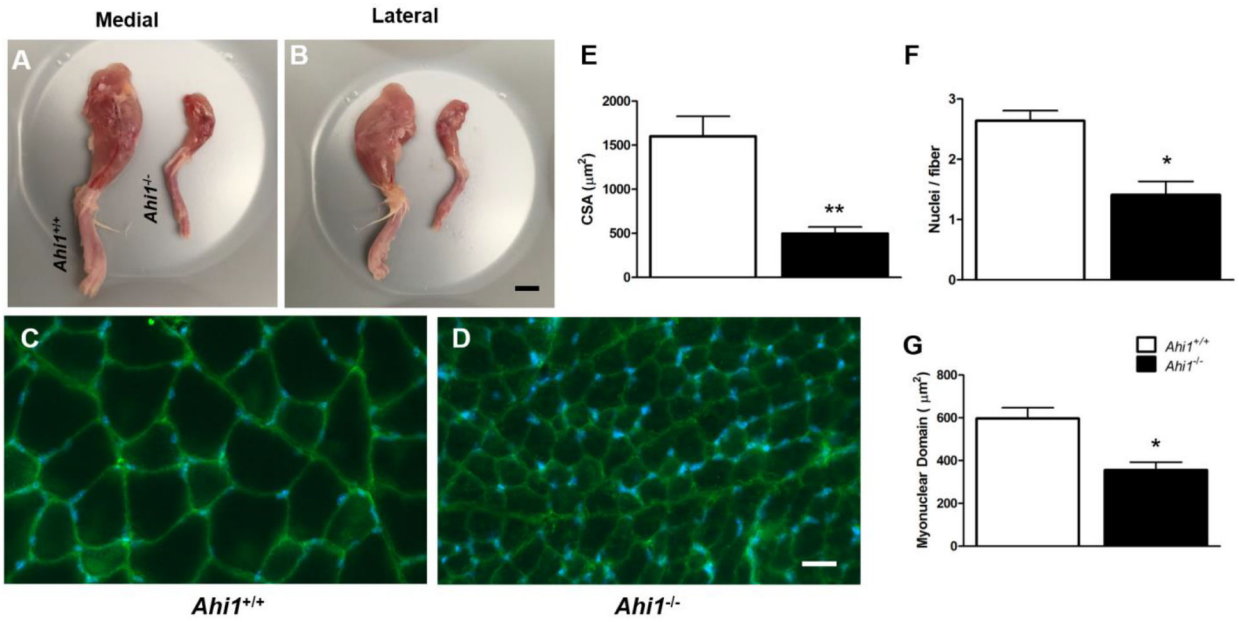

Figure 6. Reductions in hindlimb muscle mass and histological comparison of PD21 rectus femoris.

Representative medial (A) and lateral (B) views of whole hindlimb musculature show an overall reduction in muscle mass in PD21 male *Ahi1*$^{-/-}$ mice. Labeling of Na^+/K^+ ATPase α1 (green) was used to identify sarcolemma in cross section of RF in male *Ahi1*$^{+/+}$ (C) and *Ahi1*$^{-/-}$ (D) mice at PD21, revealing reduced CSA in *Ahi1*$^{-/-}$ mice (E). Quantification of nuclei also revealed reduced nuclei per muscle fiber (F) and smaller cross sectional myonuclear domain in *Ahi1*$^{-/-}$ mice (* = $P<0.05$, ** = $P<0.01$, Student's t-test; n = 3 per group). Scale bar = 5 mm (A, B); 25 μm (C, D). Data are presented as the mean ± standard error of the mean (SEM).

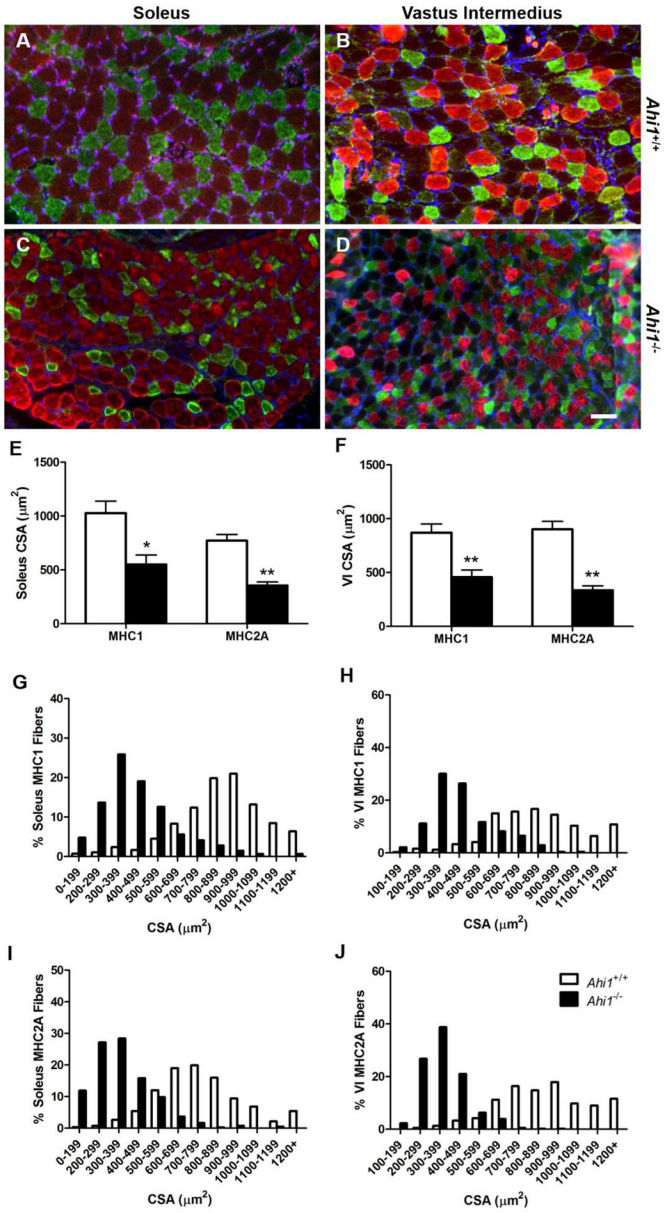

Figure 7. Reductions in cross sectional area of MHC1 and MHC2A fibers at PD21.

Cross sections of PD21 soleus (A, C) and VI (B, D) muscles show labeling of MHC Type 1 (red) and MHC Type 2A (green) fibers in *Ahi1*$^{+/+}$ (A, B) and *Ahi1*$^{-/-}$ (C, D) mice. Quantification shows reductions in the CSA of both fiber types in soleus (E) and VI (F) (* = $P<0.05$, ** = $P<0.01$, Student's t-test; n = 3 per group). (G–J) Fiber CSA distribution histograms show minimal overlap in fiber CSA between genotypes when comparing fibers of one MHC isoform within the same muscle. Data are presented as the mean ± standard error of the mean (SEM). Scale bar: 50 μm.

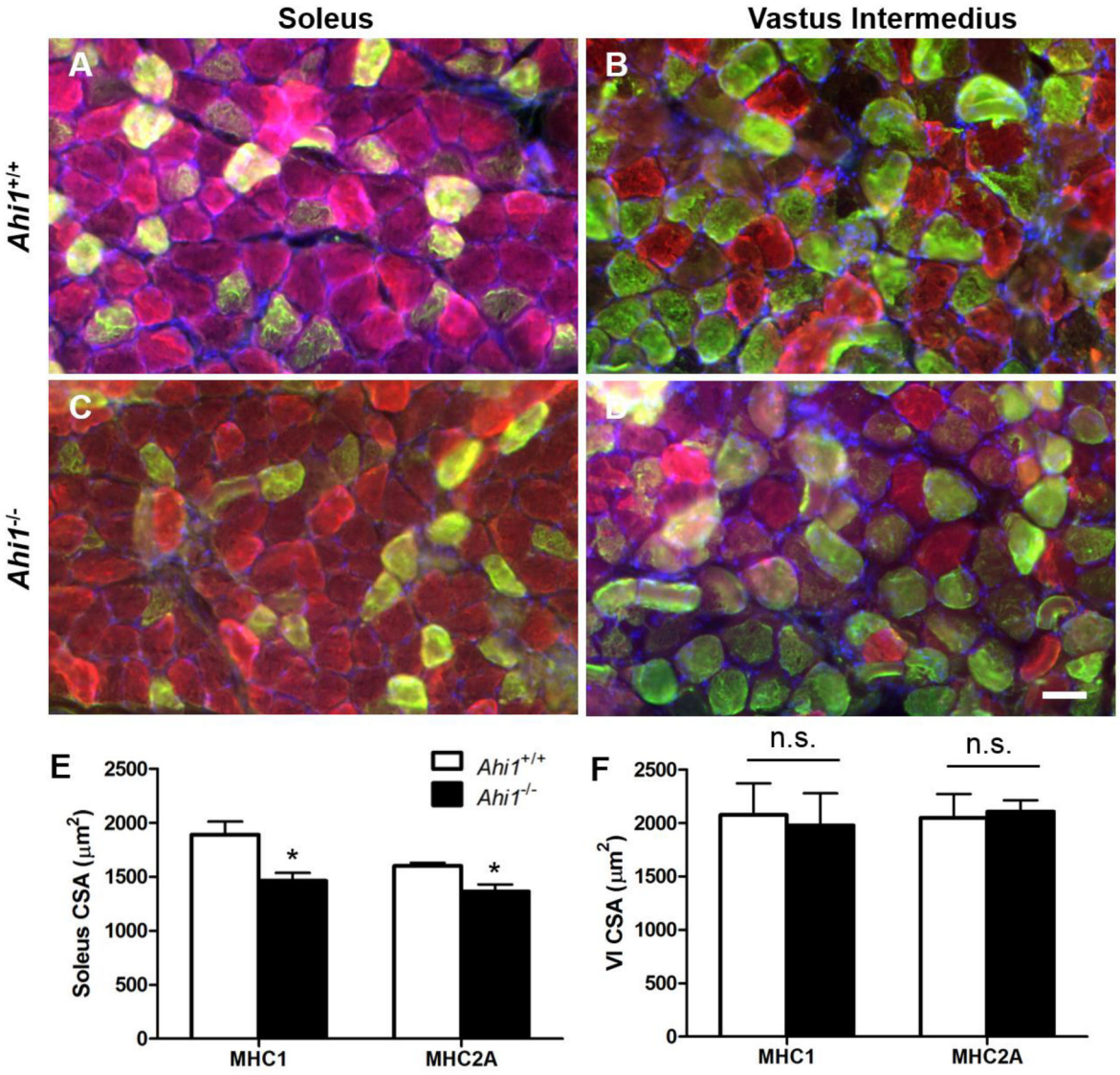

Figure 8. Fiber cross sectional area reductions in young adult mice.

Cross sections of 3-month old male soleus (A, C) and VI (B, D) muscles show labeling of MHC Type 1 (red) and MHC Type 2A (green) fibers in *Ahi1*$^{+/+}$ (A, B) and *Ahi1*$^{-/-}$ (C, D) mice. Quantification shows reductions in the CSA of both fiber types in the soleus (E), but not in the VI (F) (* = P<0.05, Student's t-test, n = 3 per group). Data are presented as the mean ± standard error of the mean (SEM). Scale bar = 50 μm.

Table 1.

Brain and muscle to body mass at PD21.

	***Ahi1*$^{+/+}$ (mg)**	***Ahi1*$^{-/-}$ (mg)**	***Ahi1*$^{+/+}$ normalized to body weight (mg/g)**	***Ahi1*$^{-/-}$ normalized to body weight (mg/g)**
Brain	422.5 ± 12.50	320.0 ± 23.09 **	29.75 ± 2.37	70.17 ± 11.52*
Gastrocnemius	62.56 ± 3.97	18.38 ± 4.44$^{\#}$	4.36 ± 0.25	3.72 ± 0.35
Soleus	9.54 ± 1.22	2.20 ± 0.37*	0.66 ± 0.07	0.48 ± 0.10
Quadriceps	67.73 ± 4.60	23.35 ± 8.25**	4.74 ± 0.34	4.45 ± 0.80

Brain and gastrocnemius, soleus, and quadriceps muscles of male PD21 mice are expressed as absolute mass and mass normalized to body mass (* = P<0.05, ** = P<0.01, # = P<0.001, Student's t-test; n = 3–4 per group). Data are presented as the mean ± SEM.